

Modeling of Continuous Casting Defects Related to Mold Fluid Flow

Brian G. Thomas, Department of Mechanical and Industrial Engineering, University of Illinois at Urbana-Champaign, Urbana, Ill. (bgthomas@uiuc.edu)

ABSTRACT

The quality of continuously cast steel is greatly influenced by fluid flow in the mold, particularly at the meniscus. Recent examples of computational model applications at the University of Illinois are presented to investigate the formation of several different types of defects related to flow phenomena. The amount of gas injection into the tundish nozzle to avoid air aspiration is quantified by modeling. Computational model calculations of superheat transport and surface-level fluctuations are presented. Meniscus defects, such as subsurface hooks and their associated inclusions, may form if the superheat contained in the steel is too low, or if top-surface-level fluctuations are too large. A thermal stress model has been used to compute the distortion of the meniscus during a level fluctuation. Gas bubbles and inclusion particles may enter the mold with the steel flowing through the submerged nozzle. In addition, mold slag may be entrained from the top surface. These particles may be removed safely into the slag layer, or may become entrapped into the solidifying shell, to form sliver or blister defects in the rolled product. Transient, turbulent flow models have been applied to simulate the transport and entrapment of particles from both of these sources. The insights gained by these modeling efforts aid greatly in the development of processing conditions to avoid the formation of these defects.

INTRODUCTION

In the continuous casting of steel, the task of the flow system is to transport molten steel at a desired flowrate from the ladle into the mold cavity and to deliver steel to the meniscus area that is neither too cold nor too turbulent. In addition, the flow conditions should minimize exposure to air, avoid the entrain-

ment of slag or other foreign material, aid in the removal of inclusions into the slag layer, and encourage uniform solidification. Achieving these somewhat contradictory tasks needs careful optimization.

Fluid flow in the mold is controlled by many design parameters and operating conditions. Nozzle geometry is the most important and includes the bore size, port angle, port opening size, nozzle wall thickness, port shape (round, oval, square), number of ports (bifurcated or multiport), and nozzle bottom design. The flow pattern also depends on parameters that generally cannot be adjusted to accommodate the flow pattern, such as the position of the flow control device (slidegate or stopper rod), nozzle clogging, casting speed, strand width and strand thickness. Fortunately, other parameters besides nozzle geometry can be adjusted to maintain an optimal flow pattern. These include the injection of argon gas, nozzle submergence depth and the application of electromagnetic forces. In choosing optimal settings for these parameters, it is important to understand how they act together to determine the flow characteristics. An increase in casting speed, for example, might be compensated by a simultaneous increase in submergence depth (or electromagnetic force), in order to maintain the same surface flow intensity. Thus, all the flow-control parameters must be optimized together as a system.

In designing the flow system, it is important to consider transients. Sudden changes are the main cause of the flow instabilities that generate surface turbulence and other problems. Because flow parameters are more easily optimized only for steady operation, each of the parameters that affects fluid flow must be carefully controlled. It is especially important to keep nearly constant the liquid steel level in the mold, powder feeding rate (to keep a constant liquid slag layer

thickness), casting speed, gas injection rate, slidegate opening, and nozzle position (alignment and submergence). It is also important to choose flow conditions that are resistant to transients and their detrimental effects, although this is difficult to predict.

Many quality problems that originate during the continuous casting of steel can be directly attributed to poor control of fluid flow conditions in the mold. ¹ In order to optimize these flow design and operation conditions, it is crucially important to understand how defects arise and how changes in the flow pattern affect those defects. This paper summarizes some of these problems and illustrates the use of computational flow models in gaining insight into them, using recent examples developed through the Continuous Casting Consortium at the University of Illinois.

DEFECTS RELATED TO FLUID FLOW

A schematic of the continuous casting process is given in Figure 1, which illustrates some of the phenomena that lead to defects due to fluid flow in the mold region of the process. Jets of molten steel are directed into the liquid by the nozzle ports and traverse across the mold cavity to impinge on the solidifying steel shell near the narrowfaces. Gas bubbles in the jet lower its density, providing lift, which may alter the flow pattern. The jets impinging against the narrowface may cause shell thinning, and even breakouts, if the superheat is too high and the interfacial gap is excessive. ² The momentum of the upward flow along the narrowfaces can raise the meniscus level there, causing a nonlinear profile along the top surface. Where this level is too high, the infiltration of liquid mold flux into the interfacial gap becomes more difficult, which can lead to nonuniform meniscus heat flux, longitudinal cracks and other surface defects.

Excessive surface turbulence may cause rapid fluctuations of the surface level. This can disrupt stable solidification at the meniscus, leading to deep oscillation marks, surface depressions, surface cracks and local entrapment of mold slag leading to delamination defects. In addition, high-speed flow across the top surface may shear droplets of liquid mold slag into the flow, where they may become entrained in the liquid steel.

On the other hand, if the surface velocities are insufficient, or if the local superheat contained in the molten steel near the meniscus is too low, then the meniscus may partially freeze to form deep oscillation marks and meniscus "hooks." These hooks are detrimental because they may entrap particles into the solidifying meniscus. Superheat also affects the nucleation and growth of equiaxed grains, which controls the solidification structure, and defects such as cen-

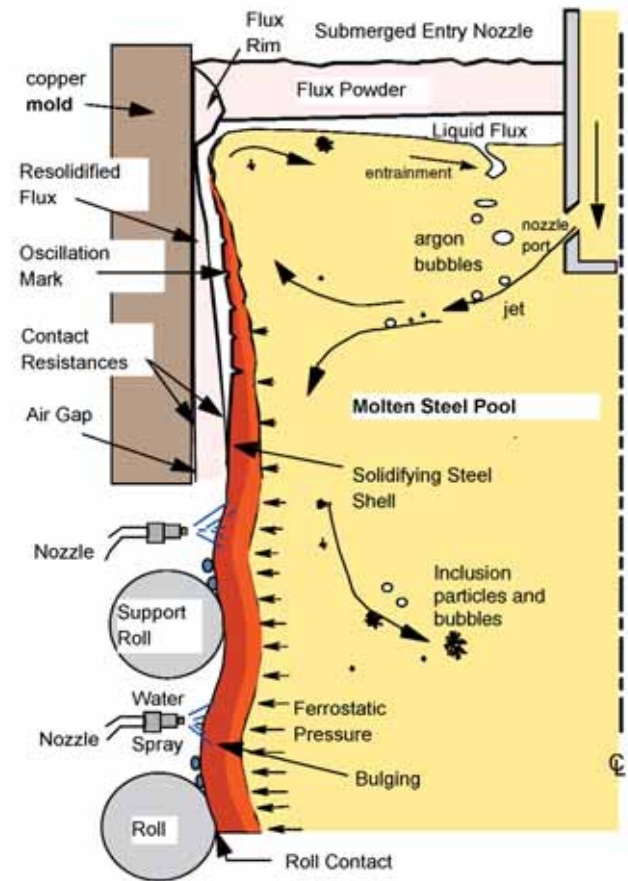


Figure 1
Flow phenomena in the continuous casting mold region.

terline segregation. The transport of solute with the fluid is also of crucial importance to macrosegregation problems, especially toward the final solidification point lower in the strand.

In addition to steel and superheat, the jets carry bubbles and inclusion particles into the mold cavity. If the flow pattern enables the particles to reach the top surface, they should be harmlessly removed into the liquid slag layer, so long as the slag is not saturated and the surface tension forces are not excessive. Alternatively, inclusions and bubbles may become entrapped in the solidifying steel shell, where they cause slivers, "pencil pipe" blisters and other costly defects. Inclusion particle behavior is complicated by their attachment to the surface of bubbles, which encourages removal, but also creates potentially dangerous large clusters, which may also be created through collisions.

COMPUTATIONAL MODELING OF FLUID FLOW

Governing Equations

Computational models to simulate fluid flow phenomena in three dimensions generally start by solving the continuity equation and Navier-Stokes equations

for incompressible Newtonian fluids, which are based on conserving mass (one equation) and momentum (three equations) at every point in a computational domain. This yields the pressure and velocity components at every point in the domain. The domain is discretized into small computational cells, which should exactly match the true shape of the flow region of the process, in this case the nozzle and liquid pool of the continuous casting mold and upper strand. When this is performed with a sufficiently refined grid to directly capture the details of the transient fluid flow pattern, this is called “direct numerical simulation.” Because this generally leads to excessive execution times, the computational grid is generally coarsened, and a “sub-grid scale model” is used to account for the effects of turbulence that occur at time and length scales smaller than an individual computational volume. This paper contains many examples using this method, which is called “large eddy simulation.”³⁻⁴ To achieve even more efficient computation on coarse grids or meshes, the effects of turbulence can be treated as an artificial increase in the fluid viscosity, which is determined by solving additional transport equations for the time-averaged flow pattern. The most popular of these Reynolds Averaged Navier Stokes, or “RANS,” methods is the $k-\epsilon$ turbulence model, which solves two additional transport equations for the turbulent kinetic energy, k , and its dissipation, ϵ .⁵ The relative advantages and accuracies of these approaches for continuous casting are compared elsewhere.⁵⁻⁶

Unless solidification is modeled together with the flow, then the shape of the liquid domain must be obtained through other means (such as a heat conduction model of shell solidification — CON1D⁷). In addition, flow through the boundaries of this domain must be imposed to satisfy the solidification rate, by specifying fixed velocity boundary conditions at the walls, as explained elsewhere.^{3,8} When course-grid RANS models are used, the thin boundary layer of the liquid is smaller than the computational cells at the walls, so they are taken into account using “turbulent wall functions.”⁶

To obtain accurate flow solutions, it is often necessary to couple the flow equations together with simultaneous solution of other equations, in order to incorporate other phenomena,⁹ such as gas injection or electromagnetic stirring/braking. For example, when a significant amount of gas is injected with the steel, its buoyancy requires a multiphase model. Many different computational approaches are possible to simulate this behavior.⁹ Ultimately, it is of crucial importance to validate the flow model predictions through comparison with measurements as much as possible, such as PIV measurements in water models.¹⁰

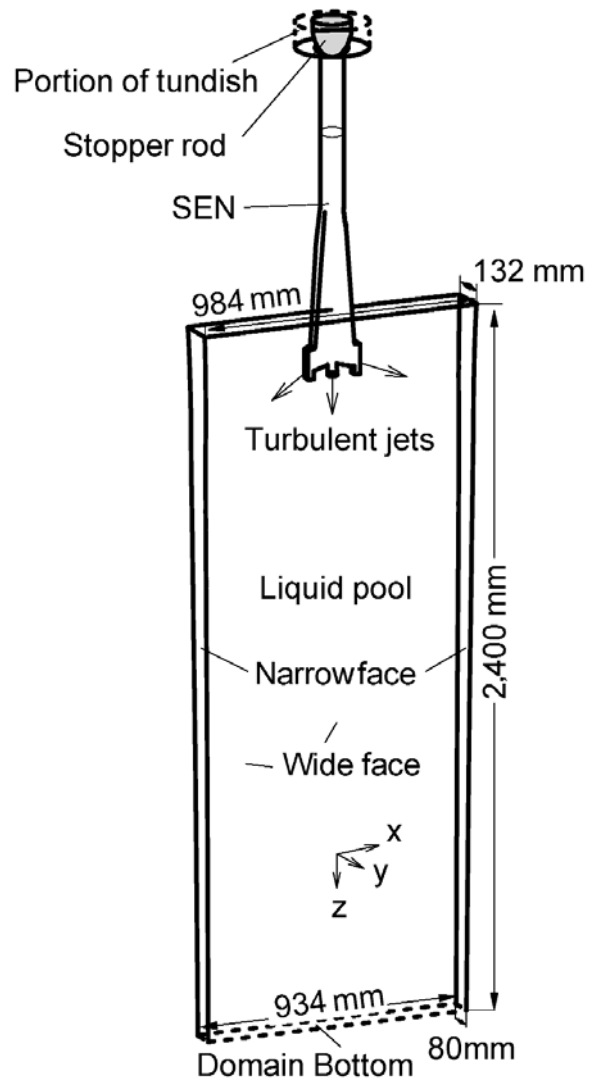


Figure 2
Schematic of the computational domain of the thin-slab steel caster, including tundish nozzle.³

Mold Geometry and Casting Conditions Studied

To illustrate the application of some of these models used to understand continuous casting defects, examples are taken from simulations conducted at the University of Illinois. For simplicity, almost all the examples involve the same thin-slab caster using the domain in Figure 2. The tapered nozzle has two 15° downward, 75 x 32 mm ports, a third round port directed straight downward, and 127-mm submergence. The straight-walled mold cavity and upper strand is 132 mm thick x 984 mm wide, cast at 1.5 m/minute with 58°C of superheat, 434 stainless steel and no gas injection. Further details are given elsewhere on the casting conditions,¹¹ computational model equations^{3,12} and experimental measurements.¹¹⁻¹²

A typical example of the fluid flow velocities in the nozzle and mold region of this thin-slab continuous caster is presented in Figure 3.³ Note the significant

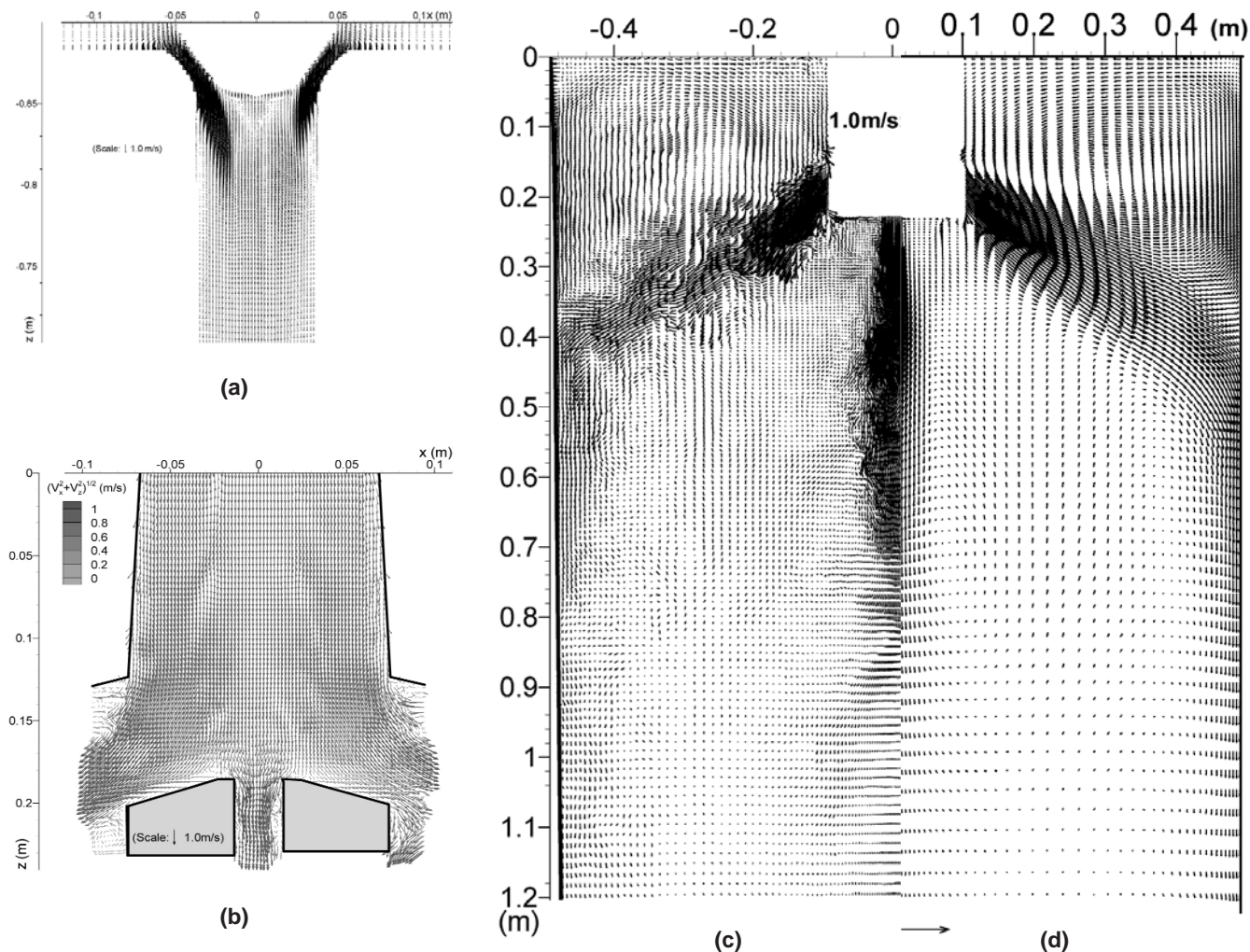


Figure 3

Computed flow pattern in the centerline between wide faces: (a) nozzle near stopper rod, (b) nozzle near exit ports, (c) instantaneous flow in the mold and (d) time-averaged flow in the mold.

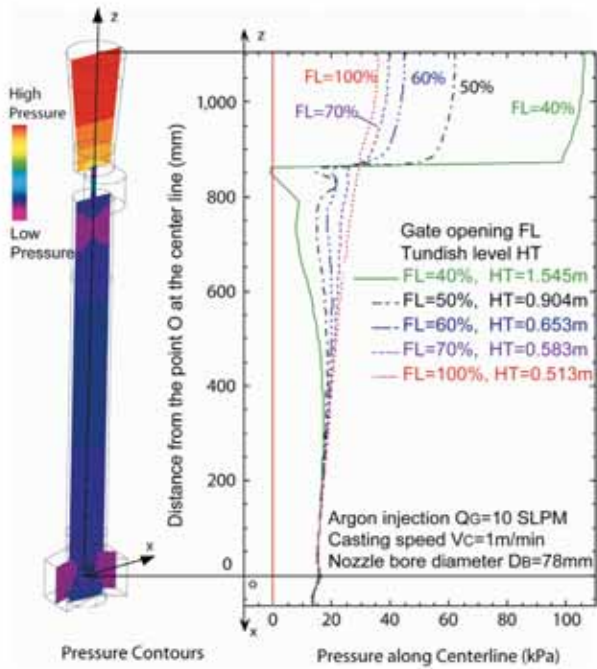
asymmetry in the instantaneous snapshot of the flow pattern in the nozzle, both around the stopper rod (Figure 3a) and at the nozzle ports (Figure 3b). Flow varies chaotically between sides, in spite of the perfectly symmetrical domain. This is characteristic of the “pseudo-steady” state of this turbulent flow, even after long-time operation. The chaotic flow continues into the mold region, as Figure 3c shows differences from the time average (Figure 3d). Generally, this example is a reasonably stable classic double-roll flow pattern. Flow impinges on the narrow faces, splits upward and downward, and traverses the top surface back toward the SEN.

MODELING OF PHENOMENA RELATED TO DEFECTS

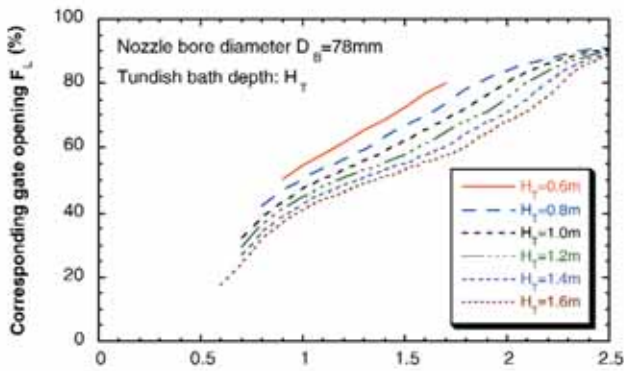
Although it is a challenging task to compute, it must be remembered that the average flow pattern itself is of no practical interest. Rather, it is a necessary first step in the simulation of related phenomena, which

depend on the fluid flow and cause defects in the steel product. With the tremendous increases in computing power and modeling sophistication, computational models are increasingly more able to simulate these important related phenomena.

One important phenomenon is the effect of argon gas injection on the pressure distribution, buoyancy, direction and pattern of the fluid flow, in both the nozzle^{13–15} and mold.^{16–17} The transport of superheat with the flow,¹⁸ and solidification of the steel shell,^{7,19} are important phenomena to meniscus hook formation, shell thinning, breakouts, internal microstructure and macrosegregation. Solute transport governs intermixing during grade changes^{20–21} and also affects segregation. Inclusion particle transport with the flow directly controls cleanliness of the product.²² Particles in the flow are subject to many forces — especially in the boundary layers near the solidification front, and at the slag-metal interface¹² — that govern entrapment of the particles into the solidification front. A



(a)



(b)

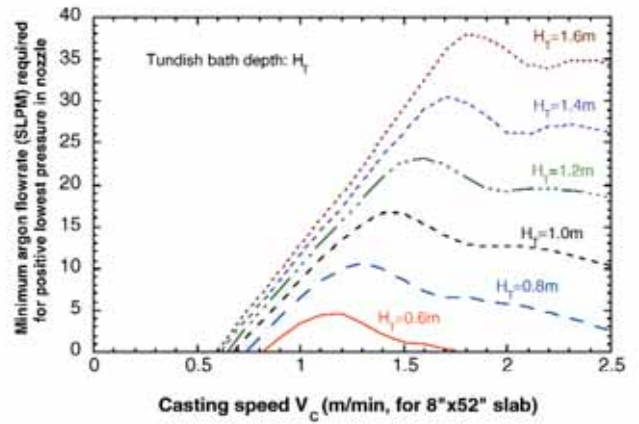
Figure 4

Pressure drop calculated down nozzle: (a) pressure contours in center plane showing that major variations are in the vertical direction, and (b) effect of slidegate opening on vertical pressure distribution.²⁴

new entrapment criterion has recently been developed and is presented elsewhere by Yuan and Thomas.¹² Other important phenomena include bulging (for the liquid pool shape changes that affect segregation) and metallurgical thermodynamics (which affects inclusion precipitation, nozzle clogging and solidification microstructure). Finally, the model must be applied in parametric studies to learn something useful about the real process.

AIR ENTRAINMENT DEFECTS

Exposure to air at any stage after steel refining leads to detrimental oxide inclusions in the steel product. This problem is worst at the final stage of flow in the mold, because there is little opportunity to prevent the

**Figure 5**

Optimizing argon gas injection (for a 78-mm bore nozzle with 90° slidegate).²⁴

reoxidation products from becoming entrapped in the final product as catastrophic large inclusions.

Open-stream pouring produces the worst air entrainment problems, which is the reason for submerged entry nozzles and mold flux operation. Air entrainment is still possible, however, if there are leaks, cracks, inadequate sealing between the nozzle joints or if the nozzle material becomes porous. If the internal pressure in the nozzle drops below atmospheric pressure, air tends to aspirate through these pathways into the nozzle. This can be identified by nitrogen pickup and dendritic inclusions from reaction in a high-oxygen environment.

Pressure in the nozzle is always lowest just below the flow control device, due to the Venturi effect of the downward-flowing metal stream. Whenever high-speed flow leaves a restricted region, such as the flow-control passage, the expanding jet tends to suck in and entrain surrounding fluid, so the pressure drops. As shown in Figure 4, the large pressure drop across the slidegate leads to a minimum-pressure region just below the slidegate, where air aspiration is most likely. For a given steel flowrate, the pressure drop (and corresponding tundish height needed to maintain the casting speed) increases as the opening is restricted, as shown in Figures 4 and 5 for a typical slidegate nozzle.¹⁵ The results in these figures were computed using a three-dimensional multiphase flow of a typical bifurcated nozzle with 15° downward, 78-mm square ports.¹⁵ The “Eulerian-Eulerian” model solves two complete sets of mass and momentum balance equations for the gas and liquid phases, which are fully coupled together through the phase fractions. The model was run many times with varying argon injection rate under feasible conditions (i.e., varying slidegate opening and casting speed together appropriately for a given tundish depth).

Air aspiration into the nozzle can be discouraged by proper introduction of an inert gas flow, which is one of the ways in which argon gas acts to prevent nozzle

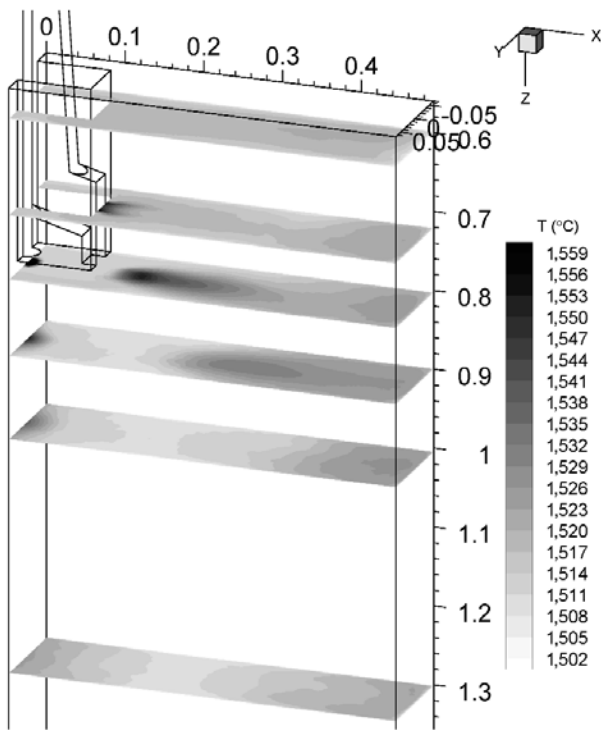


Figure 6
Temperature distribution in liquid pool (based on flow conditions in Figure 3).²⁶

clogging.²³ The addition of argon gas can replace air in feeding leaks around seals. Argon injection can also raise the minimum pressure in the nozzle above ambient.¹⁵ Note that this occurs because the slidegate must open up to accommodate the gas (shown in the top of Figure 5), in addition to the pressurizing effect of the gas. The minimum gas flowrate calculated to avoid a partial vacuum is shown at the bottom of Figure 5. When the slidegate opening is either very small or very large, the pressure never drops below 1 atmosphere (zero gauge pressure), so gas injection is not needed to prevent aspiration. Less gas is needed at low casting speed and at low tundish level, when the pressure drops are lower. Maintaining a high gas flowrate during these times may disrupt flow in the mold and thereby be detrimental to steel quality. Further insight gained from models on optimizing argon injection to avoid air entrainment is given elsewhere.¹³⁻¹⁵

SUPERHEAT TRANSPORT, SHELL THINNING AND BREAKOUTS

Impingement of the molten steel jets onto the solidifying shell in the mold can cause problems if the jet is either too hot or too cold. A jet with insufficient superheat can deliver steel to the top surface that is too cold, which leads to surface skulling, freezing of the meniscus and related surface defects, as discussed in the next section. This section focuses on problems arising if the jet is too hot. Breakouts occur when the steel shell at mold exit is not strong enough to contain

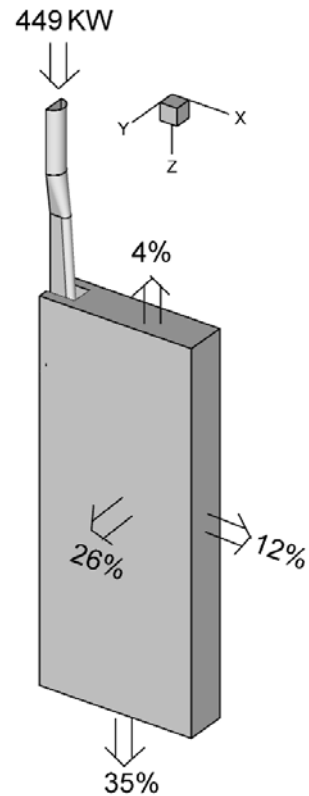


Figure 7
Superheat removal distribution (based on temperatures in Figure 6).²⁶

the liquid steel, and they have many causes. One possible cause is local thin and hot regions of the solidifying shell, which can result from high superheat dissipation at the region where an excessively hot jet impinges on the inside of the shell.^{18,25} Problems arise only if this local superheat dissipation is combined with slow heat extraction from the corresponding shell exterior. This problem is most likely in the off-corner regions, where the hot jet may impinge and the shell shrinkage also creates a larger gap.

A computational model of superheat transport has been developed for the 132-mm thin-slab caster in Figure 2.^{6,26} This computation is challenging because the thermal boundary layer has steep gradients, especially in the critical impingement region, which requires a very fine grid. The temperature contours presented in Figure 6 reveal the temperature distribution in various horizontal sections. The jet leaving the nozzle ports is hottest, and it quickly dissipates its superheat and drops in temperature as it moves through the mold. Measurements of temperature from a probe inserted into the top surface (Figure 8) agree with the predictions that roughly 70 percent of the superheat is gone at this location, which provides partial validation of the model. The predicted temperature fluctuations, indicated with the error bars, also bracket the variation in the probe measurements. Most (65 percent) of the superheat is dissipated to the

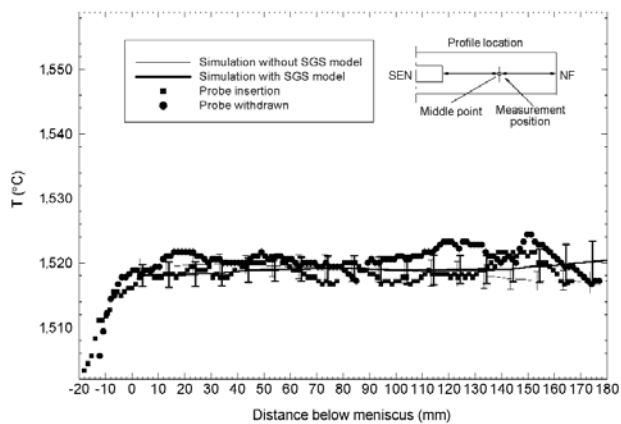


Figure 8
Comparison of simulated temperature profile and plant measurements (#3 – 295 mm from centerline).^{17,26}

shell in the mold (Figure 7), with most of the remainder dissipated just below mold exit.²⁶ As is common in slab casting with bifurcated nozzles, the impingement region on the narrowface absorbs the most superheat (12 percent) and has double the average heat flux per unit area to the wide face. Each wide faces removes 26 percent of the superheat, but its area is more than seven times larger. This high-impact region on the narrowface extends to the off-corner region of the wide faces. Heat losses through the top slag layer are small.

Figure 9 shows how shell growth depends on the combined effects of superheat input from jet impingement and heat removal to the mold walls.²⁷ Model predictions were made using CON1D — a comprehensive heat-flow solidification model of the mold, interface and shell — which features momentum, mass and force (friction) balances on the liquid flux layer.^{7,19} Jet impingement produces a thinner shell on the narrowface, compared with classic parabolic shell growth on the wide face, as shown in both the computations and measurements in Figure 9.²⁷ The importance of this shell-thinning effect increases with higher casting speeds, higher superheats and lower gap heat transfer.^{18,25} Asymmetric flow, such as that caused by nozzle clogging, may aggravate the effect.

SURFACE DEFECT FORMATION

Most surface defects in the steel product originate in the mold at the meniscus, where the solidifying steel shell is very thin. The most obvious source of surface defects is the capture of foreign particles into the solidifying shell at the meniscus. Particles come from many sources, including argon bubbles, oxide inclusions generated by prior processes that are carried in with the steel entering the mold cavity, and slag entrainment. If they are not removed by scale formation or during surface scarfing, these surface inclusions will lead to line defects or slivers in the final product. Other problems include deep oscillation

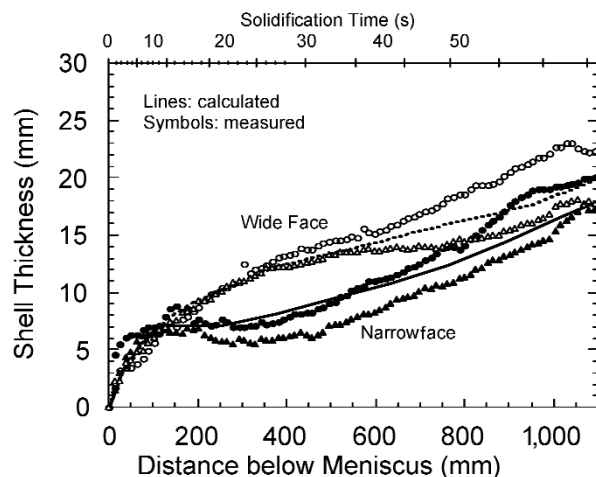


Figure 9
Breakout shell thickness profiles and corresponding model predictions, showing the thin region near location of jet impingement on narrowface, relative to steady shell growth down the wide face.²⁷

marks and surface depressions, which lower the local heat transfer, leading to a hotter local shell temperature, strain concentration and crack formation. Transverse cracks often form during unbending at the root of the deep oscillation marks. Longitudinal cracks often initiate at local hot spots around the meniscus perimeter. All these defects are worsened by large fluctuations in the top surface liquid level, which depend on the flow pattern in the mold.

Many surface defects form at the meniscus due to variations in the level of the liquid steel on the top surface of the mold cavity. These variations take two forms: a relatively steady contour across the mold width known as a “standing wave,” and “level fluctuations,” where the local level changes with time. While the standing wave can cause chronic problems with liquid slag feeding, the time-varying level fluctuations cause the most serious surface defects.

Top-surface-level Profile

The top-surface level is important because it affects the feeding of liquid flux into the interfacial gap between the mold and shell, which is important to heat transfer. Insufficient liquid flux consumption to the interfacial gap leads to increased thermal resistance, variable heat transfer, thermal stresses, stress concentration and ultimately cracks. A steep surface-level profile poses difficulty for complete coverage of the liquid flux over the steel surface. If the liquid flux layer becomes so thin that the steel surface touches the mold powder, it can become contaminated with elements such as carbon, which can cause surface quality problems such as cracks and segregation in ultralow-carbon steels.

Figure 10 shows a typical instantaneous profile of the transient top-surface level obtained from the flow field in Figure 3.^{3,28} This computation was achieved by

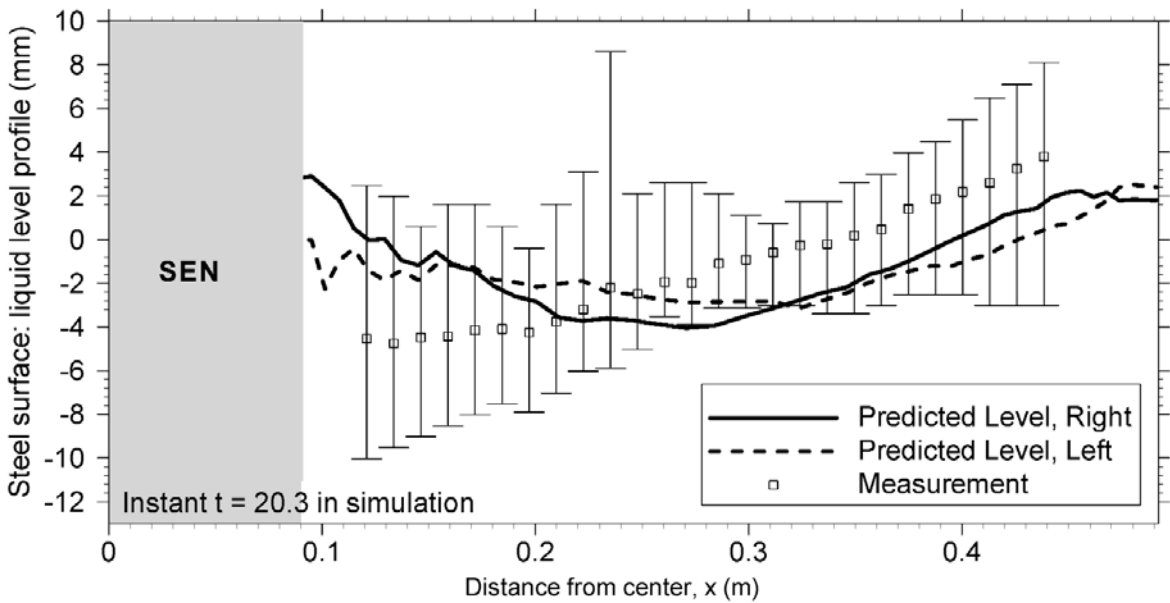


Figure 10
Comparison of predicted and measured top-surface liquid levels in steel (Figure 3 flow field).³

performing a balance between kinetic energy and potential energy on the results of pressure along the top surface. The predictions in a water model compared well with measured top-surface levels.³ The results in Figure 10 also compare with measurements of the top-surface level in the steel caster, obtained by dipping thin steel sheets. The results match within the uncertainty in the measurements (error bars), which exists regarding possible rotation of the sheets. The level is always higher near the narrowfaces, by 2 mm in the water model and by 4–6 mm in the steel caster. This is because the steel upward momentum near the narrowfaces lifts the liquid level there, displacing some of the molten flux. The flux layer must be thick enough to cover the steel, in order to provide a steady supply of molten flux into the interfacial gap to lubricate the steel. Thus, the height of the surface standing wave is important to steel quality.

Top-surface-level Fluctuations

Controlled oscillation of the mold generates ripples across the liquid level but does not present an inherent quality problem, because the liquid near the mold wall tends to move with the wall. Large, sudden jumps or dips in liquid level are much more serious.

A sudden jump in local level can cause molten steel to overflow the meniscus. In the worst case, the steel can stick to the mold wall and start a sticker breakout. Alternatively, a sudden change in level can cause an irregular extended frozen meniscus shape, or a “hook.” This defect is discussed in the next section. Variations of more than the oscillation stroke over a time interval on the order of 1 second are the most detrimental. Even low-frequency variations (over periods of more than 60 seconds) may cause defects if the

meniscus overflows and the solid slag rim is imprinted on the shell or captured.²⁹

A sudden severe drop in liquid level exposes the inside of the solidifying shell to the mold slag and also leads to surface depressions. Relaxing the temperature gradient causes cooling and bending of the top of the shell toward the liquid steel. When the liquid level rises back, the solidification of new hot solid against this cool, solid surface layer leads to even more bending and stresses when the surface layer reheats.³⁰ This sequence of events is illustrated on a 20-mm-long section of shell in the thermal-stress model results in Figure 11, for a 20- to 30-mm level drop lasting 0.6 second.³⁰ When liquid steel finally overflows the meniscus to continue with ordinary solidification, a surface depression is left behind, such as that shown in Figure 11.

The microstructural changes and surface depressions associated with level variations are serious because they initiate other quality problems in the final product. These problems include surface cracks and segregation. Surface cracks allow air to penetrate beneath the steel surface, where it forms iron oxide, leading to line defects in the final product. These defects are difficult to distinguish from inclusion-related defects, other than by the simpler composition of their oxides.

Figure 12 shows the time variation of the horizontal velocity toward the SEN at the center points between the SEN and the narrowface on the top surface. This result was obtained from the transient large eddy simulation.³ The velocity fluctuations are very large — similar to the velocity magnitude. Figure 12 shows a strong component with high frequency (e.g., flow velocity drops from ~0.4 m/second toward the

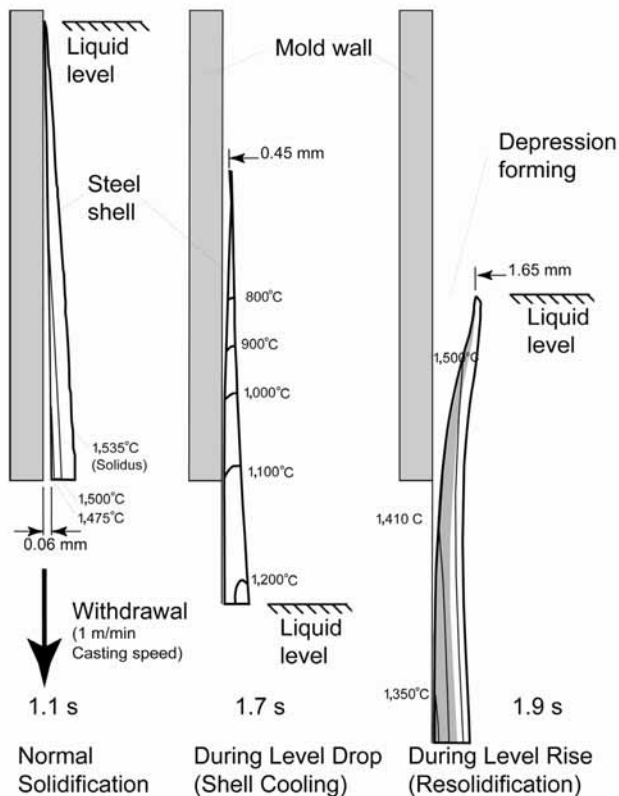


Figure 11
Events during a severe level drop (20 mm for 0.6 second) that lead to a transverse surface depression.³⁰

SEN to a velocity in the opposite direction within 0.2 second).

This prediction compares favorably with previous PIV measurements on a 0.4-scale water model.¹⁰

Simulations with and without flow across the center-line reveal that interaction between the two sides of the caster is an important cause of the large high-frequency fluctuations. This agrees with findings based on water modeling.³¹ These velocity variations are significant, because the level fluctuations that accompany them are a major cause of defects in the process. This is revealed in time-dependent animations of the profile in Figure 10.³

Hook Formation

Subsurface hook formation at the meniscus during the continuous casting of steel slabs is an important cause of surface defects, owing to their easy entrapment of mold flux and inclusion-laden gas bubbles. Figure 13 shows a typical hook, which is always associated with an oscillation mark and especially plagues ultralow-carbon steels.^{32–33} Recent work has shown that curved hooks, such as this one, form when the meniscus freezes and later overflows.³⁴ Hook shape is also affected by thermal distortion and other mechanisms.^{35–36} Hook formation is greatly affected by steel grade, superheat, level fluctuations and oscillation conditions.^{32–33}

The effect of superheat is investigated by close examination of the superheat results, shown in Figure 6,²⁶ and further application of computational models to the meniscus region. As the steel flows through the mold cavity, it continuously drops in temperature. The coldest liquid is found at the meniscus, around the perimeter of the top surface, especially near the

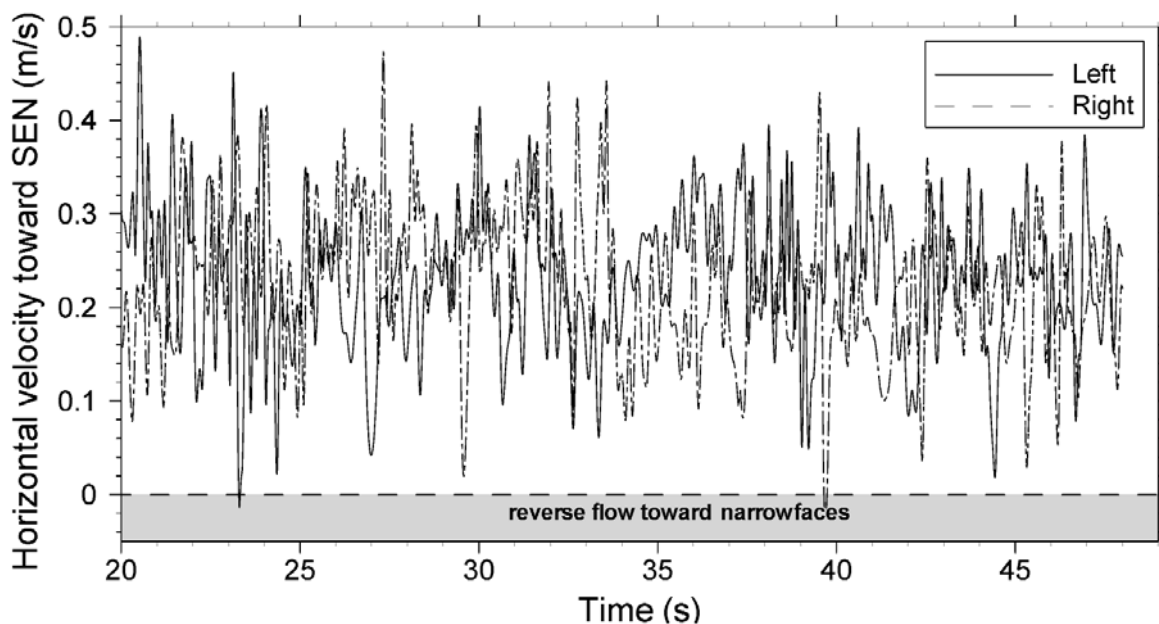


Figure 12
Time variations of the horizontal velocity toward SEN at the center point of the top surface of steel (see Figures 2 and 3).

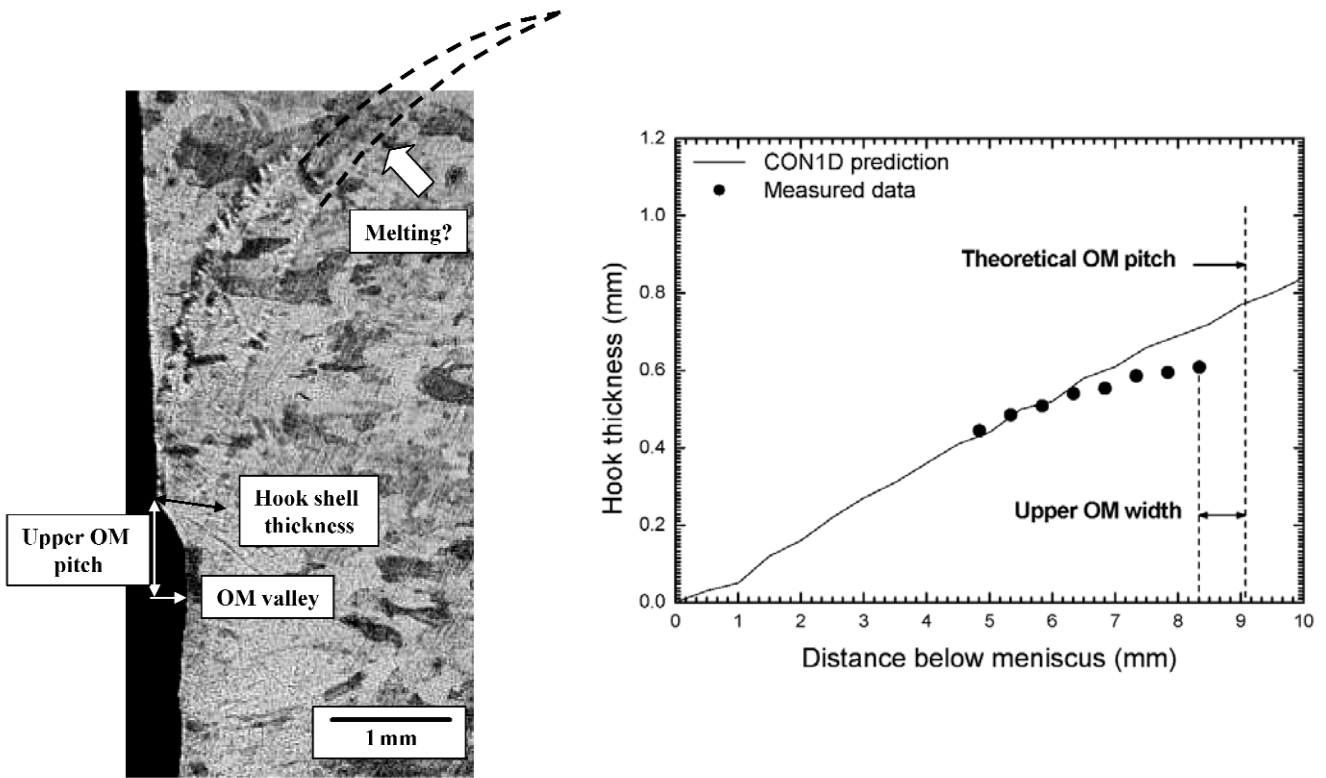


Figure 13

Typical hook shape (left) and comparison of hook-shell thickness with shell thickness prediction from CON1D (right).³³

narrowface, the wide-face centerline near the inlet nozzle, and the corners. The fluid is coldest in these places because it is both far from the inlet and stagnant. Liquid in these regions can become supercooled, causing meniscus freezing upon nucleation. In addition to forming hooks, in extreme cases, this can cause skull formation, and even “bridging,” where steel or slag freezes across the shortest distance between the nozzle and meniscus of the wide face, often leading to a breakout.

The heat flux corresponding to superheat delivery to the solidifying steel shell in the critical meniscus region is shown in Figure 14 (for slightly different casting conditions chosen to match the hook in Figure 13³⁷). The lowest superheat flux is found at the corner and near the nozzle, which coincides with the locations where the deepest meniscus hooks are observed in practice. Hooks also tend to be deeper on wide slabs with low superheat and low casting speed, for the same reasons.

Using a best estimate for superheat flux at the meniscus, the solidification of the initial shell was computed with CON1D, and the thickness compared with the measured hook shell thickness in Figure 13.³³ For the calculation, the meniscus location where the hook shell starts is taken at one theoretical oscillation mark pitch above the measured deepest part of the oscillation mark at the hook. This suggests that the hook shape revealed by etching was created

by a change in heat flow conditions that occurred due to metal overflow of the initial shell at the meniscus at the instant the oscillation mark formed. The predicted shell profile roughly matches the measured profile. The modeling results suggest that the top of

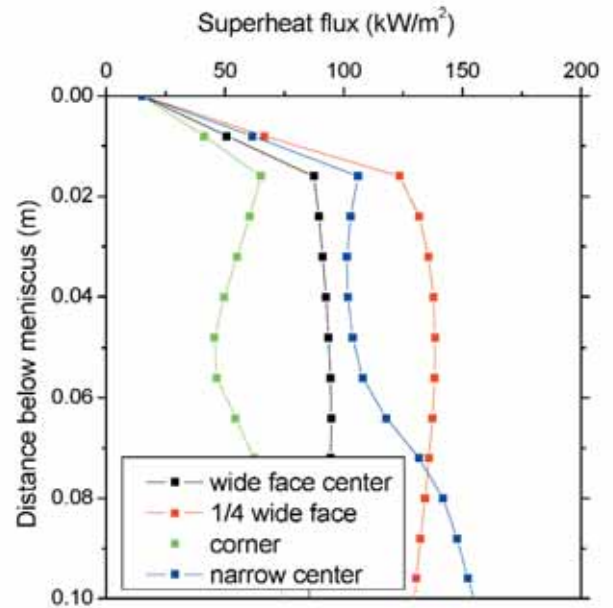


Figure 14

Variation of superheat flux (kW/m^2) in meniscus region around strand perimeter.³⁷

the original hook shell was truncated, likely due to breaking off or melting of the shell tip during the liquid overflow event. Recent metallographic evidence has proved this to indeed be the case.³⁸ Further computational efforts are being conducted to simulate the coupled phenomena governing behavior of the meniscus region, including transient fluid flow, motion of the steel/slag interface, oscillation of the mold wall and the attached slag rim, slag consumption into the gap, heat transfer in the region, and thermal distortion of the solidifying steel shell.³⁹ The results are being combined with metallographic examination and plant trails to investigate the fundamental formation mechanism of these hooks and their associated defects.

INCLUSION PARTICLE ENTRAPMENT

The entrapment of inclusions, bubbles, slag and other particles during solidification of steel products is a critical quality concern. They require expensive inspection, surface grinding and even rejection of the final product. Furthermore, if undetected, large particles lower the fatigue life, while captured bubbles and inclusion clusters cause slivers, blisters and other surface defects in rolled products. These particles have two main sources: bubbles and inclusions generated during upstream processing that enter the mold through the submerged entry nozzle, and the entrainment of mold slag from the top surface, discussed in the next section.

Particles leaving the tundish can either stick to the nozzle walls (where they lead to clogging), travel with the recirculating flow to be safely removed into the mold slag at the top surface, or become entrapped in the solidifying shell (where they lead to product defects). The fraction of particles going to each of these destinations is being quantified using a new computational model. This model first calculates the transient turbulent flow field in the mold region using large eddy simulation, with a sub-grid-scale k model.³ Next, the transport and capture of many individual particles are simulated using a Lagrangian approach to track the trajectories.⁴ The results presented here are for 30,000 particles, in order to achieve reasonable statistics. The transport equation includes the effects of six hydrodynamic forces: drag, shear lift, pressure gradient, stress gradient, added mass, and Basset history and buoyancy. The model features a new criterion to determine particle entrapment, which considers the effects of four more forces that are important in the fluid boundary layer adjacent to the solidification front. Further details on the model, including equations for the forces, are given elsewhere.^{8,12}

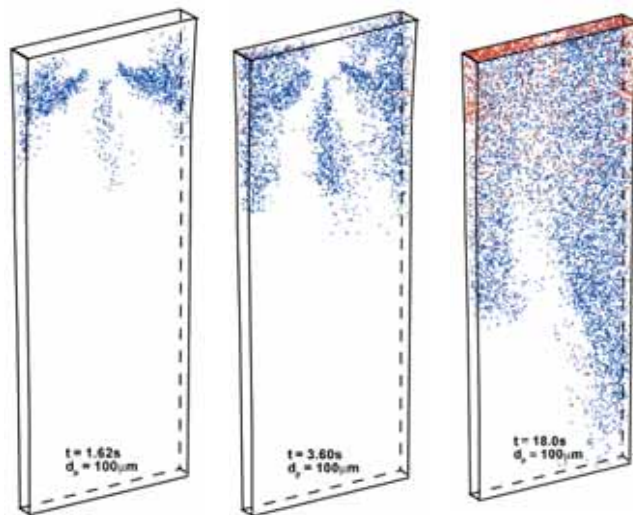


Figure 15
Transport of 100- μm inclusions in a strand at different times (red = final entrapment location, based on flow pattern in Figure 3).⁴

Instantaneous snapshots of the trajectories of 100- μm alumina inclusion particles at different times after entering in the mold region are shown in Figure 15, based on the flow pattern in Figure 3.

Note that the domain includes the 1.11-m submerged entry nozzle and the top 2.40 m of the steel



Figure 16
Final entrapment location of inclusions on stopper rod and nozzle walls (flow conditions in Figure 3).

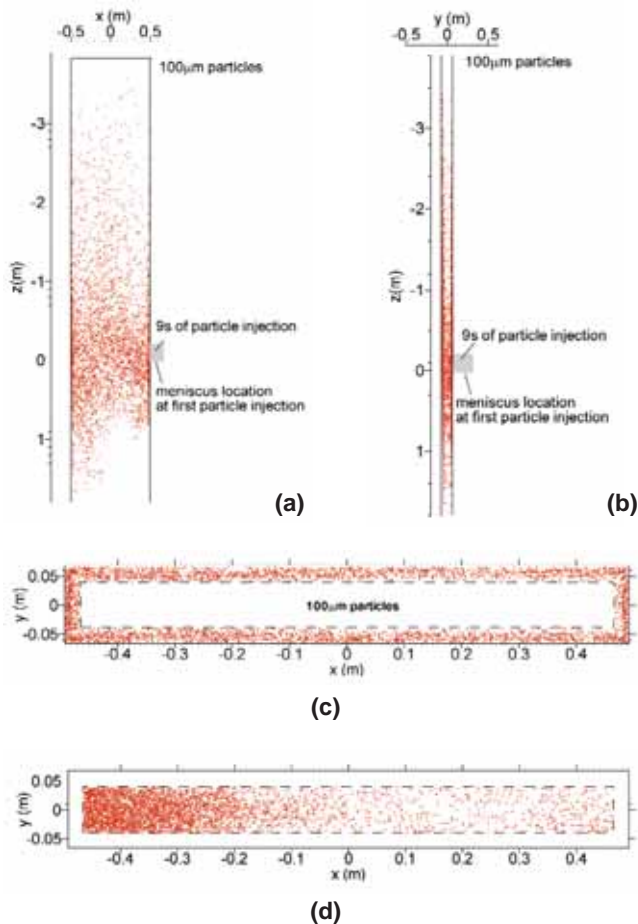


Figure 17
Particle entrapment locations predicted in the final solidified strand (based on trajectories in Figure 15): (a) wide face view, (b) narrow face view, (c) top view, and (d) top view at time of exit from domain.

strand. Particles that touch the top surface are assumed to be removed into the slag layer (and are then colored red). Note that significant asymmetry exists in the flow, which directly affects the particles, especially in the lower regions of the strand. Many more particles leave from the right side of the domain, although investigation revealed that there was no significant asymmetry at the nozzle port exit. This behavior is attributed solely to the chaotic nature of turbulence.

Nozzle Entrapment (Clogging)

The inclusion trajectories themselves are of much less practical interest than their final entrapment locations. Inclusions attaching to the nozzle walls contribute to clogging, which is detrimental to steel quality in several ways: the clogging slows production, large clogs can suddenly break off and enter the mold, and the flow pattern becomes unstable.¹⁵

An example of the predicted locations of inclusions touching the nozzle walls is shown in Figure 16. About 10 percent of the particles exiting the tundish touched the stopper rod, and a further 16 percent

touched an inner wall of the nozzle.⁸ These inclusions might stick to cause nozzle clogging in a real caster, depending on the properties of the nozzle material and thermodynamic reactions at the interface. Note that the bottom portion of the stopper rod and nearby walls of the upper nozzle have the most inclusion entrapment, which agrees with plant experience. Some particles touched the bottom of the SEN near the outlet ports.

Strand Entrapment (Sliver Defects and Blisters)

Particles traveling in the liquid pool may become entrapped in the solidifying shell to form defects. Using the new entrapment criterion, particles touching the solidification front were assumed always to become entrapped if they are smaller than the primary dendrite arm spacing. Larger particles are subjected to a force balance that considers the effects of transverse fluid flow on washing the particles away from the interface, the angle of the reaction forces between the dendrite tips, and the other hydrodynamic forces. In addition, this force balance includes the effects of the surface tension gradient, such as those caused by sulfur rejection at the solidification front, the lubrication force, and Van der Waals forces. All three of these forces tend to encourage particle entrapment and should be explored in further work. Further details on the entrapment criterion are given elsewhere.¹²

Inclusion entrapment locations in the final solidified strand were computed from the trajectory results shown in Figure 15 and are presented in Figure 17. More than 84 percent of the 100- μm inclusions were captured in the shell, including 51 percent in the upper 2.4 m of the strand. Only 8 percent touched the top slag surface, while the remaining 8 percent touched the outside of the nozzle refractory walls and might be removed. After injecting larger, 400- μm inclusions, only 30 percent were entrapped in the solidified shell. This is due both to their increased chances of flotation from their higher buoyancy, and to their smaller likelihood of capture into the solidification front.

The particles were injected through the nozzle ports during a 9-second time period, which corresponds to 0.23 m of travel of the meniscus down with the strand, and is labeled on Figure 17. The entrapment locations in the strand are distributed both upstream and downstream about this location. The side and top views (Figure 17a and b) show that the captured particles concentrate in a thin band around the strand perimeter and especially near the narrowfaces. There does not appear to be any significant concentration of particles associated with flow from the central port. Figure 17d reveals strong asymmetry in the particle

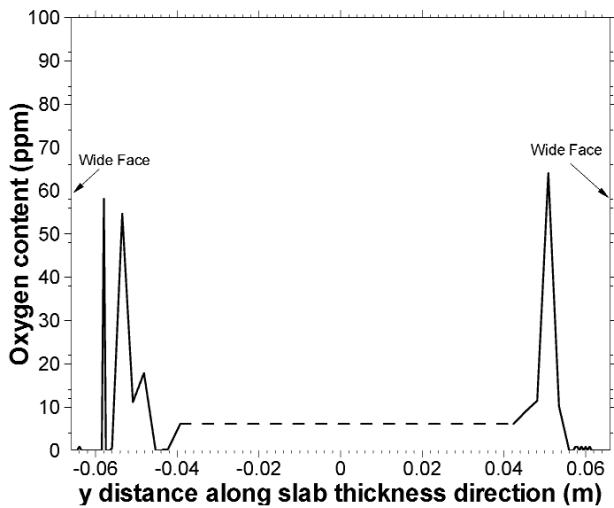


Figure 18
Oxygen content along the slab centerlines (100- μm inclusions).

trajectories through the liquid, as many more particles exit the left side of the domain into the lower strand. However, this asymmetry appears to be greatly diminished in the final entrapment locations, as Figure 17c shows much less bias toward the left side. This is because faster-moving flow across the solidification front makes capture more difficult. Capture is most likely along those regions of flow along the solidification front that move slowly downward near the casting speed. It is important to emphasize that the asymmetry is chaotic and, although the stronger flow to the left persisted for a long time interval (greater than 30 seconds), it could change to the opposite side at any time.

By reprocessing the results to model continuous inclusion injection, it is possible to compute the expected distribution of total oxygen content in an average section through the final solid strand.⁴ Figure 18 presents the results for 10 ppm total oxygen content entering from the nozzle ports in the form of 100- μm particles. Figure 18 shows that the entrapment is concentrated from 10 to 25 mm beneath the strand surface at the centerline. Considering the shell thickness profile down the strand, this region corresponds to a capture region of ~0.5–2.5 m below the meniscus. Local spikes in total oxygen in this band depend on sample size but are predicted to exceed 60 ppm, owing to grouping together of captured particles simply due to chaotic turbulence. The final entrapment position in the lower strand is uncertain, so this region is represented as a dashed line. Its average oxygen content is 6 ppm, indicating that relatively fewer particles penetrate deeper than 2.5 m below the meniscus into the lower regions of the strand.

The caster simulated here has straight vertical walls. In a curved caster, large particles in the lower recirculation zone tend to spiral toward the inner radius, with increased entrapment rates. Entrapped solid oxide

particles eventually lead to surface slivers or internal defects, which act as stress concentration sites to reduce fatigue and toughness properties of the final product. Gas bubbles captured in this way eventually may cause blister defects such as “pencil pipe,” which appear as streaks in the final rolled product. When the slab is rolled, the subsurface bubbles elongate and the layer of metal separating them from the surface becomes thinner. Later during annealing, they can expand to raise the surface of the sheet locally, especially if the steel is weak, as with ultralow-carbon grades, or if hydrogen is present.⁴⁰ Further computations are needed to quantify the expected benefits of lowering the casting speed, or using a vertical mold and the upper strand.

These results suggest that most of the inclusions that enter the mold become entrapped in the final product. Thus, nozzle design and mold operation should focus on controlling flow at the meniscus to avoid the further entrainment of new inclusions, rather than altering the flow pattern to encourage the removal of inclusions entering the mold. Upstream operations should focus on inclusion removal and reoxidation prevention.

MOLD SLAG ENTRAINMENT

Mold slag can be entrained into the solidifying shell due to vortexing, high-velocity flow that shears slag from the surface, and turbulence at the meniscus. The capture of large inclusions into the solidifying shell then leads to obvious line defects or slivers in the final product.

Vortexing most often occurs during conditions of asymmetrical flow, where steel flows rapidly through the narrow passage between the SEN and the mold. This creates swirling just beside the SEN, as shown in Figure 19.²⁶ This swirl or vortex may draw mold slag downward, near the sides of the nozzle. If it is then entrained with the jets exiting the nozzle ports, this slag will be dispersed everywhere and create defects, as discussed in the previous section. In addition to drawing in slag, the vortex is detrimental because it hastens erosion of the nozzle refractory walls. Visible erosion patterns at the locations near the off-corner and center of the wide, thin-slab nozzle have been observed in practice. In addition to the vortex, slag may also be drawn downward by the recirculation pattern that accompanies flow from the nozzle ports. Thus, slag entrapment is most likely with shallow nozzle submergence and high casting speed.

The entrainment of mold slag also occurs when the velocity across the top surface becomes high enough to shear mold slag fingers down into the flow, where they can be entrained. The breakup of the slag fingers

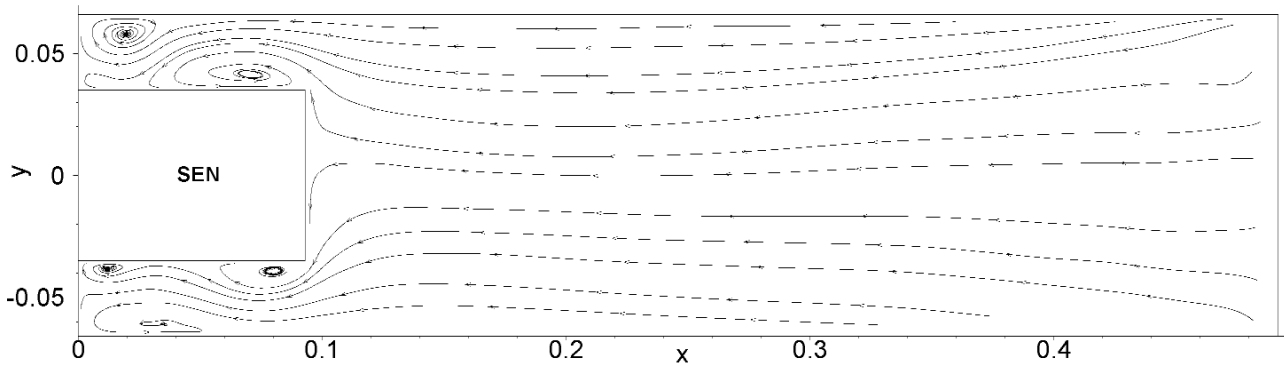


Figure 19
Velocity streamlines showing vortexing near the SEN (in-plane 38.5 mm below the top surface, flow conditions in Figure 3).²⁶

into particles is a complex process governed by surface tension, fluid properties and flow conditions. Figure 20 illustrates the transport and fate of these slag particles after they have formed.¹² Many float quickly back into the slag layer, owing to their greater buoyancy. However, many slag particles disperse into the flow and behave the same as inclusions that entered through the nozzle, eventually becoming entrapped as internal inclusion defects. Initial entrainment is easier for deeper slag layers, lower slag viscosity and lower slag surface tension.⁴¹ To avoid shearing slag in this manner, the top-surface velocity must be kept below a critical maximum value, suggested to be 0.3 or 0.4 m/second.⁴² The critical velocity may also be exceeded when the standing wave becomes too severe and the interface emulsifies.⁴³ The critical velocity also depends on the relative densities of the steel and flux phases and the mold geometry.⁴³

High-velocity surface flows also may cause emulsification of the slag, where slag and steel intermix and even create a foam if too much argon gas is present.⁴⁴ This allows easy capture of particles via vortexing or surface shearing flow. Meniscus turbulence related to level variations is another mechanism for slag entrainment, as discussed previously.

CONCLUSIONS

Fluid flow in the continuous casting process can generate many different types of defects in the final product. Computational models of fluid flow coupled with other important phenomena can be useful tools to study and quantify these problems. Several different examples of insights into defects are presented here, based on simulations conducted at the University of Illinois. These include air aspiration into the nozzle, shell thinning and breakouts from excessive superheat, surface defects from a steep "standing wave," level fluctuations, subsurface hook formation and the associated deep oscillation marks and particle entrapment, and the entrapment into the solidifying shell of inclusion particles and bubbles

entering the nozzle or from mold slag entrainment at the top surface.

ACKNOWLEDGMENTS

The author wishes to thank his former students, especially Q. Yuan, B. Zhao and H. Shin, and research scientist L. Zhang for their efforts generating the results sampled in this paper. This work was supported by the National Science Foundation (Grant #DMI-01-15486) and the Continuous Casting Consortium at

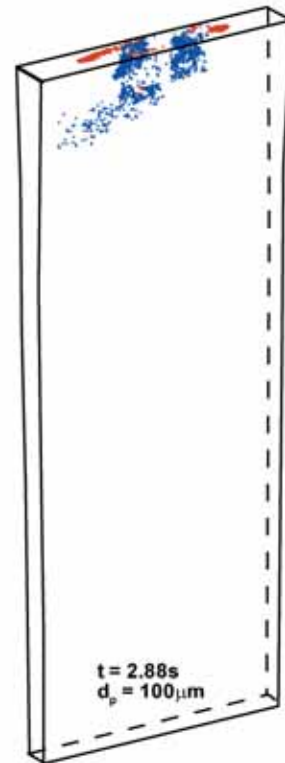


Figure 20
Instantaneous snapshot of the distribution of 100- μm slag particles, just after entrainment into the top surface (red indicates particles that refloated, while blue indicates particles that are still moving, flow conditions in Figure 3).

the University of Illinois. Thanks are also given to the National Center for Supercomputing Applications at the University of Illinois for computing time.

REFERENCES

1. Thomas, B.G., "Chapter 14: Fluid Flow in the Mold," *The Making, Shaping and Treating of Steel: Continuous Casting*, edited by A. Cramb, AISE Steel Foundation, Pittsburgh, Pa., 2003, pp. 14.1–14.41.
2. Thomas, B.G.; Moitra, A.; and McDavid, R., "Simulation of Longitudinal Off-corner Depressions in Continuously Cast Steel Slabs," *ISS Transactions*, Vol. 23 (4), 1996, pp. 57–70.
3. Yuan, Q.; Thomas, B.G.; and Vanka, S.P., "Study of Transient Flow and Particle Transport During Continuous Casting of Steel Slabs, Part 1: Fluid Flow," *Metall. & Material Trans. B.*, Vol. 35B (4), 2004, pp. 685–702.
4. Yuan, Q.; Thomas, B.G.; and Vanka, S.P., "Study of Transient Flow and Particle Transport During Continuous Casting of Steel Slabs, Part 2: Particle Transport," *Metall. & Material Trans. B.*, Vol. 35B (4), 2004, pp. 703–714.
5. Thomas, B.G.; Yuan, Q.; Sivaramakrishnan, S.; Shi, T.; Vanka, S.P.; and Assar, M.B., "Comparison of Four Methods to Evaluate Fluid Velocities in a Continuous Casting Mold," *ISIJ International*, Vol. 41 (10), 2001, pp. 1266–1276.
6. Yuan, Q.; Zhao, B.; Vanka, S.P.; and Thomas, B.G., "Study of Computational Issues in Simulation of Transient Flow in Continuous Casting," *Steel Research International*, Vol. 76 (1), 2005, pp. 33–43.
7. Meng, Y., and Thomas, B.G., "Heat Transfer and Solidification Model of Continuous Slab Casting: CON1D," *Metall. & Material Trans.*, Vol. 34B (5), 2003, pp. 685–705.
8. Yuan, Q., "Transient Study of Turbulent Flow and Particle Transport During Continuous Casting of Steel Slabs," Ph.D. thesis, University of Illinois at Urbana-Champaign, Ill., 2004.
9. Thomas, B.G., and Zhang, L., "Review: Mathematical Modeling of Fluid Flow in Continuous Casting," *ISIJ International*, Vol. 41 (10), 2001, pp. 1181–1193.
10. Yuan, Q.; Sivaramakrishnan, S.; Vanka, S.P.; and Thomas, B.G., "Computational and Experimental Study of Turbulent Flow in a 0.4-scale Water Model of a Continuous Steel Caster," *Metall. & Material Trans.*, Vol. 35B (5), 2004, pp. 967–982.
11. Thomas, B.G.; O'Malley, R.J.; and Stone, D.T., "Measurement of Temperature, Solidification, and Microstructure in a Continuous Cast Thin Slab," *Modeling of Casting, Welding, and Advanced Solidification Processes*, edited by B.G. Thomas and C. Beckermann, San Diego, Calif., TMS, Warrendale, Pa., Vol. VIII, 1998, pp. 1185–1199.
12. Yuan, Q., and Thomas, B.G., "Transport and Entrapment of Particles in Continuous Casting of Steel," *ICS 2005 — 3rd International Congress on Science and Technology of Steelmaking*, Charlotte, N.C., May 9–12, 2005.
13. Bai, H., and Thomas, B.G., "Turbulent Flow of Liquid Steel and Argon Bubbles in Slide-Gate Tundish Nozzles, Part I: Model Development and Validation," *Metall. & Material Trans. B.*, Vol. 32B (2), 2001, pp. 253–267.
14. Bai, H., and Thomas, B.G., "Turbulent Flow of Liquid Steel and Argon Bubbles in Slide-Gate Tundish Nozzles, Part II: Effect of Operation Conditions and Nozzle Design," *Metall. & Material Trans. B.*, Vol. 32B (2), 2001, pp. 269–284.
15. Bai, H., and Thomas, B.G., "Effects of Clogging, Argon Injection and Continuous Casting Conditions on Flow and Air Aspiration in Submerged Entry Nozzles," *Metall. & Material Trans. B.*, Vol. 32B (4), 2001, pp. 707–722.
16. Thomas, B.G.; Huang, X.; and Sussman, R.C., "Simulation of Argon Gas Flow Effects in a Continuous Slab Caster," *Metall. Trans. B.*, Vol. 25B (4), 1994, pp. 527–547.
17. Shi, T., "Effect of Argon Injection on Fluid Flow and Heat Transfer in the Continuous Slab Casting Mold," master's thesis, University of Illinois at Urbana-Champaign, 2001.
18. Huang, X.; Thomas, B.G.; and Najjar, F.M., "Modeling Superheat Removal During Continuous Casting of Steel Slabs," *Metall. Trans. B.*, Vol. 23B (6), 1992, pp. 339–356.
19. Meng, Y., and Thomas, B.G., "Interfacial Friction-related Phenomena in Continuous Casting With Mold Slags," *Metall. & Material Trans. B.*, Vol. 34B (5), 2003, pp. 707–725.
20. Huang, X., and Thomas, B.G., "Intermixing Model of Continuous Casting During a Grade Transition," *Metall. Trans. B*, Vol. 27B (4), 1996, pp. 617–632.
21. Thomas, B.G., "Modeling Study of Intermixing in Tundish and Strand During a Continuous Casting Grade Transition," *Iron & Steelmaker*, Vol. 24 (12), 1997, pp. 83–96.
22. Sussman, R.C.; Burns, M.; Huang, X.; and Thomas, B.G., "Inclusion Particle Behavior in a Continuous Slab Casting Mold," *Iron & Steelmaker*, Vol. 20 (2), 1993, pp. 14–16.
23. Rackers, K.G., and Thomas, B.G., "Clogging in Continuous Casting Nozzles," *Continuous Casting Vol. 10: Tundish Operations*, Iron & Steel Society, Warrendale, Pa., 2003, pp. 264–274.
24. Bai, H., "Argon Bubble Behavior in Slide-Gate Tundish Nozzles During Continuous Casting of Steel Slabs," Ph.D. thesis, University of Illinois at Urbana-Champaign, 2000.
25. Lawson, G.D.; Sander, S.C.; Emling, W.H.; Moitra, A.; and Thomas, B.G., "Prevention of Shell Thinning Breakouts Associated With Widening Width Changes," *Steelmaking Conference Proceedings*, Vol. 77, Chicago, Ill., 1994, Iron & Steel Society, Warrendale, Pa., pp. 329–336.
26. Zhao, B., "Numerical Study of Heat Transfer in Continuous Casting of Steel," master's thesis, University of Illinois at Urbana-Champaign, 2003.
27. Thomas, B.G.; O'Malley, R.; Shi, T.; Meng, Y.; Creech, D.; and Stone, D., "Validation of Fluid Flow and Solidification Simulation of a Continuous Thin Slab Caster," *Modeling of Casting, Welding, and Advanced Solidification Processes*, Vol. IX, Shaker Verlag GmbH, Aachen, Germany, Aug. 20–25, 2000, pp. 769–776.

28. Yuan, Q.; Thomas, B.G.; and Vanka, S.P., "Turbulent Flow and Particle Motion in Continuous Slab Casting Molds," *ISSTech 2003 Process Technology Proceedings*, Vol. 86, Indianapolis, Ind., April 27–30, 2003, Iron & Steel Society, Warrendale, Pa., pp. 913–927.
29. Thomas, B.G.; Jenkins, M.; and Mahapatra, R.B., "Investigation of Strand Surface Defects Using Mold Instrumentation and Modeling," *Ironmaking & Steelmaking*, Vol. 31, 2004, pp. 485–494.
30. Thomas, B.G., and Zhu, H., "Thermal Distortion of Solidifying Shell in Continuous Casting of Steel," *Proceedings of Internat. Symposia on Advanced Materials & Tech. for 21st Century*, Honolulu, Hawaii, edited by I. Ohnaka and D. Stefanescu, TMS, Warrendale, Pa., 1996, pp. 197–208.
31. Honeyands, T., and J. Herbertson, "Flow Dynamics in Thin Slab Caster Moulds," *Steel Research*, Vol. 66 (7), 1995, pp. 287–293.
32. Shin, H-J.; Lee, G.G.; Choi, W.Y.; Kang, S.M.; Park, J.H.; Kim, S.H.; and Thomas, B.G., "Effect of Mold Oscillation on Powder Consumption and Hook Formation in Ultralow-carbon Steel Slabs," *AISTech 2004 Proceedings*, Nashville, Tenn., Sept. 15–17, 2004, AIST, Warrendale, Pa.
33. Shin, H-J.; Thomas, B.G.; Lee, G.G.; Park, J.M.; Lee, C.H.; and Kim, S.H., "Analysis of Hook Formation Mechanism in Ultralow-carbon Steel Using CON1D Heat Flow Solidification Model," *MS&T'04*, New Orleans, La., Sept. 26–29, 2004, TMS, Warrendale, Pa., Vol. II, 2004, pp. 11–26.
34. Sengupta, J.; Thomas, B.G.; Shin, H-J.; Lee, G.G.; and Kim, S.H., "Mechanism of Hook Formation During Continuous Casting of Ultralow-carbon Steel Slabs," *Metallurgical and Materials Transactions A* (in press), 2006.
35. Sengupta, J., "Effect of a Sudden Level Fluctuation on Hook Formation During Continuous Casting of UltraLow Carbon Steel Slabs," *Modeling of Casting, Welding, and Advanced Solidification Processes XI*, Opio, France, May 28–June 2, 2006, edited by C.A. Gandin and J.E. Allison, TMS, Warrendale, Pa., 2006.
36. Sengupta, S., and Thomas, B.G., "Thermomechanical Effects Near the Meniscus During Continuous Casting of Ultralow-carbon Steel," *MS&T'05*, Pittsburgh, Pa., Sept. 26, 2005, TMS, Warrendale, Pa.
37. Zhang, L.; Sengupta, J.; and Thomas, B.G., "Investigation of Meniscus Hook Formation Using Computational Models," final report to Postech, University of Illinois, 2004.
38. Sengupta, J.; Shin, H-J.; Thomas, B.G.; and Kim, S.H., "Micrograph Evidence of Meniscus Solidification and Subsurface Microstructure Evolution in Continuous Cast Ultralow-carbon Steels," *Acta Materialia*, Vol. 54 (4), 2005, pp. 1165–1173.
39. Ojeda, C.; Sengupta, J.; Thomas, B.G.; Barco, J.; and Arana, J.L., "Mathematical Modeling of Thermal Fluid Flow in the Meniscus Region During an Oscillation Cycle," *AISTech 2006 Conference Proceedings*, May 1–4, 2006, Cleveland, Ohio, AIST, Warrendale, Pa.
40. Abbel, G.; Damen, W.; de Gendt, G.; and Tiekink, W., "Argon Bubbles in Slabs," *ISIJ International*, Vol. 36, 1996, pp. S219–S222.
41. Harman, J.M., and Cramb, A.W., "A Study of the Effect of Fluid Physical Properties Upon Droplet Emulsification," *Steelmaking Conference Proceedings*, Dallas, Texas, Vol. 79, Iron & Steel Society, Warrendale, Pa., 1996, pp. 773–784.
42. Kubota, J.; Okimoto, K.; Shirayama, A.; and Murakami, H., "Meniscus Flow Control in the Mold by Travelling Magnetic Field for High-speed Slab Caster," *Mold Operation for Quality and Productivity*, edited by A.W. Cramb and E. Szekeres, Iron & Steel Society, Warrendale, Pa., 1991.
43. Theodorakakos, A., and Bergeles, G., "Numerical Investigation of the Interface in a Continuous Steel Casting Mold Water Model," *Metall. & Material Trans. B*, Vol. 29B (6), 1998, pp. 1321–1327.
44. Emling, W.H.; Waugaman, T.A.; Feldbauer, S.L.; and Cramb, A.W., "Subsurface Mold Slag Entrainment in Ultralow-carbon Steels," *Steelmaking Conference Proceedings*, Chicago, Ill., Vol. 77, Iron & Steel Society, Warrendale, Pa., 1994, pp. 371–379. ♦

The original version of this paper was presented at ICS 2005 — The 3rd International Congress on the Science and Technology of Steelmaking, Charlotte, N.C., and published in the ICS 2005 Proceedings.